Published in final edited form as:
*Chem Sci*. 2020 April 21; 11(15): 3986–3995. doi:10.1039/D0SC00738B.

# Transforming colloidal $Cs_4PbBr_6$ nanocrystals with poly(maleic anhydride-*alt*-1-octadecene) into stable $CsPbBr_3$ perovskite emitters through intermediate heterostructures†

**Dmitry Baranov**[*,a], **Gianvito Caputo**[a], **Luca Goldoni**[b], **Zhiya Dang**[a], **Riccardo Scarfiello**[c], **Luca De Trizio**[a], **Alberto Portone**[d], **Filippo Fabbri**[d], **Andrea Camposeo**[d], **Dario Pisignano**[d,e], **Liberato Manna**[*,a]

[a]Nanochemistry Department, Istituto Italiano di Tecnologia, Via Morego 30, 16163 Genova, Italy

[b]Analytical Chemistry Lab, Istituto Italiano di Tecnologia, Via Morego 30, 16163 Genova, Italy

[c]CNR NANOTEC, Institute of Nanotechnology, c/o Campus Ecotecne, via Monteroni, 73100 Lecce, Italy

[d]NEST, Istituto Nanoscience-CNR, Piazza S. Silvestro 12, I-56127 Pisa, Italy

[e]Dipartimento di Fisica “Enrico Fermi”, Università di Pisa, Largo Bruno Pontecorvo 3, I-56127 Pisa, Italy

## Abstract

The preparation of strongly emissive $CsPbBr_3$ perovskite nanocrystals with robust surface passivation is a challenge in the field of lead halide perovskite nanomaterials. We report an approach to prepare polymer-capped $CsPbBr_3$ perovskite nanocrystals by reacting oleylammonium/oleate-capped $Cs_4PbBr_6$ nanocrystals with poly(maleic anhydride-*alt*-1-octadecene) (PMAO). PMAO contains succinic anhydride units that are reactive towards the oleylamine species present on the $Cs_4PbBr_6$ nanocrystals' surface and produces polysuccinamic acid, which, in turn, triggers the $Cs_4PbBr_6$ to $CsPbBr_3$ conversion. The transformation occurs through the formation of $Cs_4PbBr_6$–$CsPbBr_3$ heterostructures as intermediates, which are captured because of the mild reactivity of PMAO and are investigated by high-resolution electron microscopy. The $Cs_4PbBr_6$–$CsPbBr_3$ heterostructures demonstrate a dual emission at cryogenic temperature with an indication of the energy transfer from $Cs_4PbBr_6$ to $CsPbBr_3$. The fully-transformed $CsPbBr_3$ NCs have high photoluminescence quantum yield and enhanced colloidal stability, which we attribute to the adhesion of polysuccinamic acid to the NC surface through its multiple functional groups in place of oleate and alkylammonium ligands. The PMAO-induced transformation of $Cs_4PbBr_6$ NCs opens up a strategy for the chemical modification of metal halide NCs initially passivated with nucleophilic amines.

dmitry.baranov@iit.it; liberato.manna@iit.it.

**Author contributions**
The manuscript was written through the contributions of all authors. All authors have given approval to the final version of the manuscript.

**Conflicts of interest**
The authors declare no competing financial interest.


Europe PMC Funders Author Manuscripts

## Introduction

Nanocrystals (NCs) of cesium lead halides have recently emerged as a class of semiconductor materials promising for light-emitting applications.[1–3] The chemical reactivity of these NCs and the interconversion between the NCs of the two most studied bromides in this class, $Cs_4PbBr_6$ and $CsPbBr_3$ perovskite, have been of interest since these NCs were first synthesized in the colloidal form.[4–8] The $Cs_4PbBr_6 \rightarrow CsPbBr_3$ conversion, which can be triggered using various reagents (for example, Prussian blue,[9] oleic acid,[10] $PbBr_2$,[7,11] and water)[12–14] is an interesting approach to prepare emissive $CsPbBr_3$ NCs. For example, Yin's group exploited heterogeneous water-mediated CsBr extraction from $Cs_4PbBr_6$ NCs in hexane as a method for making luminescent $CsPbBr_3/SiO_2$ or $CsPbBr_3/Ta_2O_5$ Janus-type heterostructures,[13] and branched $CsPbBr_3$ dodecapods.[15] Despite several reports on $Cs_4PbBr_6 \rightarrow CsPbBr_3$ transformation at the nanoscale, the nanocrystal intermediates of this reaction and the surface passivation and stability of the resulting $CsPbBr_3$ NCs have not been investigated.

Designing the $Cs_4PbBr_6 \rightarrow CsPbBr_3$ NC transformation in such a way that it delivers encapsulated $CsPbBr_3$ NCs with an enhanced stability is a promising approach for exploiting the $Cs_4PbBr_6$ NC reactivity, as shown by the above mentioned studies of Yin's group.[13] The use of an organic polymer instead of an inorganic oxide (*e.g.* $SiO_2$ or $Ta_2O_5$) shell would yield a NC-polymer blend which can be drop-cast, spin-coated or electrospun, widening the range of available applications.[16] More generally, polymer encapsulation of $CsPbX_3$ perovskite NCs (X = Cl, Br, I, and their mixtures) is promising because it has been shown to enhance the shelf-time of NCs by providing enhanced stability against moisture and photodegradation.[17] Interestingly, stability enhancement has been reported irrespective of whether polymer chains preserve the native $CsPbX_3$ NC surface ligands as in the case of polystyrene[17–19] and poly(styrene– ethylene–butylene–styrene),[17] or whether the polymer adheres to the surface of $CsPbX_3$ NCs as in the case of ammonium bromide-terminated polystyrene[20] or poly(*n*-butyl methacrylate) modified with zwitterionic sulfobetaine or phosphorylcholine functional groups.[21] Arguably, an ideal NC transformation of $Cs_4PbBr_6 \rightarrow CsPbBr_3$ in this context could be caused by a polymer which acts both as a reactant and a macromolecular surfactant,[20] minimizing the number of reagents and preparatory steps involved in the process.

In this work, we demonstrate that poly(maleic anhydride-1-*alt*-octadecene) (PMAO) can simultaneously trigger the $Cs_4PbBr_6 \rightarrow CsPbBr_3$ NC transformation and provide enhanced surface passivation to the resulting $CsPbBr_3$ NCs. PMAO is a widely available co-polymer of 1-octadecene and maleic anhydride and has been extensively used for the surface functionalization of NCs.[22–24] In our experiments, upon mixing PMAO with oleylammonium/oleate-capped $Cs_4PbBr_6$ NCs, the cyclic anhydride groups of PMAO react with oleylamine species, forming polysuccinamic acid (Fig. 1). Polysuccinamic acid destabilizes the NC surface by displacing both the amine and the oleate ligands and acidifies the reaction environment, thus triggering the formation of $CsPbBr_3$ NCs (Fig. 1). The core chemistry of the NC transformation is summarized by the following chemical equation: $Cs_4PbBr_6 + n RNH_2 + (–R'(CHCO)_2O–)_n \rightarrow CsPbBr_3 + (-R'(CHCOOH)(CHCONHR)-)_n + 3Cs^+_{(solvated)} + 3Br^-_{(solvated)}$, where R = oleyl, R'= octadecenyl, and the ratio between

oleylamine molecules and anhydride units is assumed to be 1 : 1 for simplicity. The extent of the transformation is tunable by varying the amount of added PMAO, enabling the investigation of the transformation intermediates, which consist of $Cs_4PbBr_6$–$CsPbBr_3$ heterostructures. The fully-transformed $CsPbBr_3$ NCs are bright emitters and retain their green emission for four weeks of storage under ambient conditions in air, even after one washing cycle with ethyl acetate (a solvent which typically causes the degradation of oleylammonium/oleate-capped $CsPbBr_3$ NCs within hours or days). The increase in the stability of $CsPbBr_3$ NCs synthesized from $Cs_4PbBr_6$ and PMAO is attributed to the adhesion of polysuccinamic acid to the NC surface through its multiple functional groups.

## Results and discussion

### $Cs_4PbBr_6$ NCs and their transformation with PMAO in solution

The synthesis of the initial $Cs_4PbBr_6$ NCs was performed in air, *via* the hot injection of cesium oleate into the solution of lead(II) bromide dissolved in a mixture of oleylamine and oleic acid in 1-octadecene,[7] as detailed in Section S1 of the ESI.† The synthesis is similar to that of $CsPbBr_3$ NCs,[5] except that it is performed at a higher concentration of oleylamine and oleic acid with respect to lead ([oleylamine] : [oleic acid] : [$PbBr_2$] ~0.63 : 0.31 : 0.027 M). Such reaction conditions favor the formation of a Pb-poor $Cs_4PbBr_6$ phase over the $CsPbBr_3$ phase, as detailed previously.[25] The synthesis delivers batches of Csrich rhombohedral $Cs_4PbBr_6$ NCs with a narrow size distribution and an average diameter in the range from 10 to 16 nm (Fig. 2a, b, and S1–S5†). $^1H$ and $^1H$–$^{13}C$ heteronuclear single quantum coherence (HSQC) nuclear magnetic resonance (NMR) experiments established that $Cs_4PbBr_6$ NCs are passivated by a mixture of oleylammonium oleate and neutral oleylamine with a ligand ratio of ~3 : 2 between (oleylamine + oleylammonium) : oleate species (see Section S3 and Fig. S6–S9 of the ESI for details†).

These $Cs_4PbBr_6$ NCs can react with PMAO in toluene, fully or partially transforming into $CsPbBr_3$ NCs, depending on the amount of the added polymer (Fig. 2c). The reaction of $Cs_4PbBr_6$ NCs with PMAO typically starts within a few minutes after the addition of PMAO at room temperature (Movie S1 and Fig. S10†) and can be accelerated by mild heating of the reaction mixture (up to 80 °C). It is important to highlight here that heating up the NCs alone to 80 °C without the addition of PMAO does not trigger any transformation (Fig. S11†). The fully-transformed $CsPbBr_3$ NCs have a narrow size distribution, as inferred from their self-organization into ordered close-packed monolayers on a carbon-coated TEM copper grid (Fig. 2a). The XRD patterns of the initial NCs, partially- and completely-transformed samples are shown in Fig. 2b. Following the transformation, the XRD reflections of the rhombohedral $Cs_4PbBr_6$ crystal structure gradually disappeared, and peaks characteristic of the orthorhombic $CsPbBr_3$ perovskite phase emerged (Fig. 2b, see Fig. S12† for peak assignment). The progression of the reaction was monitored by steady-state UV-Vis absorption spectroscopy (Fig. 2c, left panel, Fig. S10†) in which the disappearance of the ~314 nm peak characteristic of $Cs_4PbBr_6$ [7] and the appearance of the ~510 nm band edge absorption of $CsPbBr_3$ are evident. The transformation was also tracked by steady-state photo-luminescence (PL) spectroscopy, through the appearance of a cyan emission ($\lambda_{max}$ ~475–480 nm) in the early stages of the reaction (Fig. S10†). The absolute PL quantum

Europe PMC Funders Author Manuscripts

yield (PLQY) of the samples transformed in air was measured to be ~19% (partially transformed), and ~25% (fully transformed). On the other hand, when the transformation was performed under an inert atmosphere, the sample had a 69% PLQY (Fig. S13–S15†). Such a value is comparable to those reported for other $Cs_4PbBr_6 \rightarrow CsPbBr_3$ chemical transformations of NCs: 47% (ref. 7) and 62% (ref. 11) *via* the addition of solid $PbBr_2$ at elevated temperatures, and 75% (ref. 12) upon reaction with $H_2O$. The lower PLQY of the samples transformed in air is attributed to the presence of electron traps formed as a result of sample exposure to atmospheric $O_2$. Similar results have been reported by Rodà *et al.* who observed PL dimming in oxygen-exposed $CsPbBr_3$ nanocubes.[26]

## Rationalization of the observed reactivity between PMAO and $Cs_4PbBr_6$ NCs

PMAO is a copolymer of octadecene-1 and maleic anhydride, and it consists of repeating units composed of a saturated hydrocarbon chain and a cyclic succinic anhydride ring (Fig. 1). PMAO has a negligible reactivity towards inorganic salts such as $Cs_4PbBr_6$, as confirmed in a control experiment on finely ground powder of bulk $Cs_4PbBr_6$ (Fig. S16 and S17†). However, the succinic anhydride rings of PMAO feature acyl groups that are reactive towards nucleophilic reagents such as water and primary amines (yielding, in the latter case, either succinamic acid at room temperature[23,29–31] or cyclic imides at high temperatures[31–33]). The presence of a significant amount of water as a potential reactant towards PMAO in the $Cs_4PbBr_6$ NC samples was ruled out based on FTIR and NIR characterization (Fig. S18 and S19†). On the other hand, the ligand shell of $Cs_4PbBr_6$ NCs contains partially-protonated oleylamine (Section S3 and Fig. S6–S9†). In analogy with the widely studied oleylammonium/oleate-capped $CsPbBr_3$ NCs,[25,34–36] the ligands on the surface of $Cs_4PbBr_6$ NCs are likely to exist in a dynamic equilibrium between neutral and protonated species (oleylamine and oleylammonium, respectively). Thus neutral oleylamine is always available in the NC solution. Neutral oleylamine is a nucleophile with a documented reactivity towards linear and cyclic anhydrides,[37,38] and polymaleic anhydride derivatives.[39,40] The reaction between neutral oleylamine and PMAO in the absence of NCs causes broadening of the vinyl hydrogen resonance of the oleyl chain in the $^1H$ NMR spectrum due to the attachment of small oleylamine molecules to PMAO macromolecules (the specified $M_w$ of PMAO is ~30 000–50 000 g $mol^{-1}$, which roughly corresponds to ~80–150 succinic anhydride-octadecene subunits) (Fig. S20–S22†). The addition of neutral oleylamine to cyclic anhydride produces a succinamic acid derivative, as was confirmed by $^1H$ and $^1H$–$^{13}C$ HSQC NMR in a control reaction (Fig. S23†). Therefore, the formation of polysuccinamic acid (Fig. 1) is expected upon mixing of PMAO with oleylammonium/oleate capped $Cs_4PbBr_6$ NCs. The key role of oleylamine species in the $Cs_4PbBr_6 \rightarrow CsPbBr_3$ NC transformation was further verified by a control reaction between PMAO and oleylamine-free $Cs_4PbBr_6$ NCs (synthesized with tri*n*-octylphosphine oxide (TOPO) and oleic acid[41]). The $Cs_4PbBr_6$ NCs synthesized with TOPO and oleic acid were found to be unreactive towards PMAO (Fig. S27 and S28†).

In summary, the removal of oleylamine from the surface of $Cs_4PbBr_6$ NCs destabilizes them, while polysuccinamic acid acidifies the reaction environment. Surface destabilization and acidic environments are both general conditions that are known to cause the $Cs_4PbBr_6 \rightarrow CsPbBr_3$ transformation.[10,25,42] The stoichiometry of the transformation is balanced by a

nominal removal of 3 equivalents of CsBr from 1 equivalent of $Cs_4PbBr_6$, yet we have not experimentally detected crystalline CsBr by XRD or high-resolution TEM (HRTEM). This discrepancy is tentatively rationalized by solvation of $Cs^+$ and Br ions by oleate and polysuccinamic acid species, similar to the previously reported dissociation of CsBr in dimethylformamide in the presence of the polyacrylic acid co-polymer.[43] Eventually, our $^1H$ NMR analysis also revealed that the final NCs were capped solely by polysuccinamic acid, indicating the displacement of both the oleate and amine/ammonium ligands from the NC surface upon transformation (see the discussion in Section S9 and Fig. S20–S26†).

## Enhanced stability of the $CsPbBr_3$/PMAO NCs

The fully-transformed $CsPbBr_3$ NCs formed an optically clear solution in toluene. These $CsPbBr_3$ NCs possessed an enhanced stability compared to the polymer-free, ligand-capped $CsPbBr_3$ NCs directly synthesized by following the cesium oleate/lead(II) bromide route.[5,25] Such enhanced stability was demonstrated by the fact that the NCs retained their green emission after four weeks of storage under ambient conditions in air (Fig. S29†), even after undergoing a washing cycle of precipitation/redispersion with ethyl acetate (Fig. S30 and S31†), while the polymer-free $CsPbBr_3$ NCs aggregated within hours or days after undergoing a similar washing procedure. Another indicator of the increased stability is the observation that the $CsPbBr_3$/PMAO NCs could be concentrated or diluted over ~5 orders of magnitude range of concentrations, from ~26 mg $ml^{-1}$ to ~$1 \times 10^{-4}$ mg $ml^{-1}$, without any loss of optical transparency or PL emission (Fig. S32†). The increase in the stability of the fully-transformed $CsPbBr_3$/PMAO NCs is in agreement with prior reports on $CsPbBr_3$ NCs blended with PMAO[44,45] or with the related dodecyl-grafted-poly(isobutylene-*alt*-maleic-anhydride).[46] Our hypothesis is that the binding of polysuccinamic acid through its multiple functional groups to the NC surface, in place of the standard ligands used in the direct synthesis of $CsPbBr_3$ NCs (as discussed above and in Section S9, Fig. S20–S26†), is the origin of this enhancement. To test this hypothesis, we compared the solvodynamic diameters of PMAO and $CsPbBr_3$/PMAO NCs (washed once with ethyl acetate) determined by dynamic light scattering (~1.7 ± 1.2 nm and ~11.2 ± 0.9 nm, respectively, Fig. S33 and S34†) with the sizes of the inorganic $CsPbBr_3$ cores from the TEM analysis of the same sample (~7 nm edge length, Fig. S35†). The larger solvodynamic diameter of $CsPbBr_3$/PMAO NCs in solution compared to the $CsPbBr_3$ NC edge length from TEM is explained by the PMAO wrapping and NC tumbling in solution (the diagonal of a cube with a 7 nm edge length is ~12 nm). The lack of a substantial increase in the solvodynamic diameter of $CsPbBr_3$/PMAO NCs is interpreted as an indicator of PMAO wrapping around NCs, supporting the hypothesis about the origin of increased NC stability. In addition, the relatively small solvodynamic diameter of $CsPbBr_3$/PMAO NCs indicates that PMAO molecules do not bind multiple NCs together.

## $Cs_4PbBr_6$–$CsPbBr_3$ heterostructures

The $Cs_4PbBr_6 \rightarrow CsPbBr_3$ NC transformation with PMAO is relatively slow at room temperature. This enabled the observation of NC intermediates consisting of $Cs_4PbBr_6$–$CsPbBr_3$ heterostructures (Fig. 3), which were investigated by HRTEM (Fig. 3a–e). In one of the partially-transformed samples we observed NCs with different degrees of conversion (Fig. 3a–e). The heterostructures displayed a variety of interfaces between $Cs_4PbBr_6$ and

$CsPbBr_3$, some adopting an epitaxial relationship, some not (analysis of the cases is shown in Fig. S36†). For example, the heterostructure shown in Fig. 3c, analyzed in detail in Fig. 3f–h, is characterized by an epitaxial relationship adopted by the two domains, as indicated by the overlap of the spots from the planes of the two crystal structures in fast Fourier transform (FFT, Fig. 3g) of the real space image. The < 5% mismatch between the atomic spacing of the two domains $\left[d(\overline{312})_{CsPbBr_3} = 2.37\text{Å},\ d(\overline{630})_{CS_4PbBr_6} = 2.29\text{Å}\right]$ leads to a slight bending of the planes, as labeled by the dashed lines in Fig. 3f. This bending also indicates that the atomic planes of $Cs_4PbBr_6$ domains on the two sides of the $CsPbBr_3$ domain are rotated by a small angle. The rotation gives rise to extended diffraction spots in the FFT image, instead of single sharp spots that would otherwise appear for a single crystal. Considering an orthorhombic phase for $CsPbBr_3$ (ICSD: 97851, $a$ = 8.207Å, $b$ = 8.255 Å, $c$ = 11.759 Å), the epitaxial relationship between the two domains can be described as follows: $CsPbBr_3$ [021]k$Cs_4PbBr_6$ [001], and $CsPbBr_3$ (112)k$Cs_4PbBr_6$ (030) (see Fig. 3h).

The low-magnification TEM images of the two NC samples were analyzed to quantify changes in the NC dimensions before and after the transformation (Fig. S37–S42†). For example, a sample of 10.1 nm ± 1.4 nm diameter $Cs_4PbBr_6$ NCs transformed into 8 nm ± 0.4 nm edge length $CsPbBr_3$ NCs (Fig. 2a). The Scherrer analysis of the XRD patterns of the same sample before and after the transformation indicated a reduction in the crystallite size from 16.1 ± 1.8 nm to 12.5 ± 2.6 nm, in agreement with the TEM analysis (larger dimensions from XRD as compared to TEM are due to the differences between techniques and analyses). In another sample, 15.7 nm ± 2.6 nm $Cs_4PbBr_6$ NCs transformed into 12 nm ± 1.9 nm NCs (dimensions from TEM). If one assumes that such transformation does not proceed by dissolution–recrystallization, but simply by the gradual removal of CsBr from each individual spherical NC of $Cs_4PbBr_6$, converting it to a cube-shaped NC of $CsPbBr_3$, then by volume contraction the resulting $CsPbBr_3$ NCs should have an edge length of 6 nm in TEM (9.5 nm in the second sample), which is ~2 nm smaller than the obtained value (Table S1†). Hence, dissolution–recrystallization processes should also play an important role in this transformation. A similar mechanism has been previously invoked to rationalize the inverse NC transformation (from $CsPbBr_3$ to $Cs_4PbBr_6$).[8,10]

The PL of the partially-converted sample containing $Cs_4PbBr_6$–$CsPbBr_3$ heterostructures was surveyed at room and cryogenic temperatures (see Section S14 of the ESI† for experimental details) because their optical properties are unknown to date. The results are presented in Fig. 4a and b as excitation-emission maps (PL maps). The room temperature ($T$ ~292 K) PL map of the partially-converted sample contains a single emission peak of $CsPbBr_3$ at ~504 nm (Fig. 4a). The $CsPbBr_3$ emission has a broad PL excitation spectrum (inset in Fig. 4a) with a dip at ~314 nm characteristic of $Cs_4PbBr_6$ absorption. Upon cooling to $T$ ~35 K, the PL map shows two emission peaks (Fig. 4b): an intense peak at ~513 nm and a weak peak at ~376 nm (inset in Fig. 4b). The ~513 nm peak is an emission feature of $CsPbBr_3$, red-shifted from ~504 nm as a result of cooling.[48,49] The ~376 nm emission with narrow excitation at ~313 nm is assigned to $Cs_4PbBr_6$ because it matches with previously reported cryogenic PL spectra of bulk $Cs_4PbBr_6$ (ref. 50) and $Cs_4PbBr_6$ aggregates in CsBr.[51] This assignment was further confirmed by collecting the PL map of the as-synthesized $Cs_4PbBr_6$ NCs at $T$ ~27 K (Fig. S43†). At 27 K, the emission of the as-synthesized

$Cs_4PbBr_6$ NCs is dominated by a peak at ~376 nm surrounded by weaker features due to various electronic transitions in $Pb^{2+}$ ions.[52–54] The as-synthesized $Cs_4PbBr_6$ NCs are not emissive at room temperature and, besides the discussed ~376 nm emission, are non-emissive up to the detection limit of 1600 nm when cooled (Fig. S44†).

The dual emission of partially-transformed NCs provides an opportunity to probe the energy transfer between $Cs_4PbBr_6$ and $CsPbBr_3$. Fig. 4c shows a comparison between pairs of emission spectra for the partially-converted sample collected at two different temperatures (292 K and 35 K) and two different excitation energies: one matching with $Cs_4PbBr_6$ absorption ($\lambda_{exc}$ ~ 312 nm) and one below it ($\lambda_{exc}$ ~ 402 nm, only $CsPbBr_3$ absorbs). At 292 K (Fig. 4c, left panel), only $CsPbBr_3$ emits, regardless of excitation energy, and its emission is quenched by a factor of ~2.3 after changing the excitation energy from ~402 nm to ~312 nm. This quenching is attributed to the attenuation of ~312 nm excitation due to absorption by $Cs_4PbBr_6$ and an excitation-dependent PL efficiency.[55] At 35 K, both materials emit, and the $CsPbBr_3$ emission is quenched by a smaller factor of ~1.3 (Fig. 4c, right panel). We can assign the lower quenching of $CsPbBr_3$ emission at 35 K to the energy transfer from $Cs_4PbBr_6$, which indeed is favored due to the overlap between the emission of the donor ($Cs_4PbBr_6$) and the absorption of the acceptor ($CsPbBr_3$). These initial observations make $Cs_4PbBr_6$–$CsPbBr_3$ NCs a promising platform for future spectroscopic studies of the energy flow between lead halide perovskites and related compounds.

## Reactivity of $Cs_4PbBr_6$ NC samples with PMAO in drop-cast films

The reaction described above can also proceed inside a polymer film (as was confirmed by *in situ* Raman spectroscopy, see Fig. S45†), which makes its investigation relevant for the emerging application of blends between PMAO and oleylammonium/oleate-capped perovskite NCs in light-emitting diodes.[44,45] From this point of view, the $Cs_4PbBr_6$ to $CsPbBr_3$ transformation is an indicator of amine-anhydride reactivity, and its kinetics can be studied *in situ* by steady-state and time-resolved PL. Fig. 5 shows the results of the *in situ* PL measurements from a macroscopic area (~2 mm excitation spot size) of the film made by quick drop-casting of a freshly prepared PMAO–$Cs_4PbBr_6$ NCs blend. Green PL develops within the first few minutes in the drop-cast film, and reaches a stable intensity and position (~510 nm, full width at half maximum of 18 nm) after ~2 hours (Fig. 5a and b), indicating the timescale of the complete conversion. Both the PL intensity and the absorbance of the film (at 405 nm, the wavelength of the CW laser used for excitation) increase over the course of the transformation, with a characteristic time constant of about ~10 minutes (Fig. 5c). Similar kinetics were obtained by *in situ* micro-PL performed with a confocal fluorescence microscope (Fig. S46†), suggesting that the transformation proceeds uniformly across the blend. The PLQY in the film remains almost constant at ~20% throughout the transformation, similar to the values measured in the solution (Fig. 5d).

The evolution of PL during the transformation was also monitored by *in situ* spectrally-resolved transient PL. The temporal PL decay is sub-ns and contains two main components, the shorter (~70 ps) and longer (950 ps) ones (Fig. 5e and S47†). The shorter decay component varies little over the course of the transformation while the longer decay component decreases from ~1.1 ns to ~800 ps with a time constant of 10 minutes (Fig. 5f).

The PL decay of the emitting NCs in the film is much shorter than that of the NCs in solution (~4–5 ns), the polymer-free $CsPbBr_3$ NCs[5,35,56–58] (~2–10 ns), and polymer-encapsulated single $CsPbBr_3$ NCs (~6 ns).[18] It is definitely much shorter than that of $MAPbBr_3$ NCs/polymer blends (>100 ns).[59] The fast PL decay of $CsPbBr_3$/PMAO NCs in the drop-cast film can be attributed to various possible causes, including: (i) the appearance of a new non-radiative carrier recombination channel, ascribable to oxygen molecules (as the samples were prepared in air) which act as traps for electrons;[26] (ii) electron hopping between neighboring nanocrystals in the film;[60] (iii) a more defective surface of NCs formed in films, due to reduced mobility of ions and molecules (preventing efficient passivation of surface sites in comparison to the solution case). The sub-ns PL decay of NCs in blends with PMAO, combined with a reasonable PLQY, should be of interest for applications in scintillators, where ultrafast and efficient emission is required for fast timing capability of imaging detectors.[61,62]

## Conclusions

Chemical transformation of colloidal $Cs_4PbBr_6$ NCs to perovskite $CsPbBr_3$ NCs induced by the organic co-polymer PMAO is presented as a promising strategy to prepare stable and bright $CsPbBr_3$ NC emitters. The PMAO reactivity towards oleylammonium/oleate-capped $Cs_4PbBr_6$ NCs favors an addition reaction of oleylamine ligands from the NC surface to the succinic anhydride groups of the polymer. This destabilizes the NCs and acidifies the reaction environment through the formation of polysuccinamic acid, a PMAO–oleylamine adduct, which binds to the surface of the NCs *in lieu* of the original ligands. These two factors – ligand replacement and *in situ* acid formation – drive the $Cs_4PbBr_6$ to $CsPbBr_3$ NC transformation. The lower reactivity of PMAO, as compared to that of the previously reported reagents, enabled the investigation of $Cs_4PbBr_6$–$CsPbBr_3$ intermediate heterostructures by HRTEM. The heterostructures feature a variety of epitaxial and non-epitaxial relationships between the two structurally dissimilar domains. At cryogenic temperature, $Cs_4PbBr_6$–$CsPbBr_3$ NCs display dual emission at ~376 nm and 513 nm with evidence of energy transfer from $Cs_4PbBr_6$ to $CsPbBr_3$. The PMAO-induced transformation proceeds both in solutions and in drop-cast films, producing $CsPbBr_3$ NCs with a narrow size distribution and attractive photoluminescence properties (up to 69% PLQY in solution and a sub-ns PL lifetime in the drop-cast films). The resulting $CsPbBr_3$/PMAO NCs demonstrate enhanced stability by retaining their green emission for several weeks in air. The increased stability of $CsPbBr_3$/PMAO NCs is attributed to the adhesion of polysuccinamic acid through its multiple functional groups to the NC surface. The PMAO-induced transformation of $Cs_4PbBr_6$ NCs opens up a general strategy for chemical modification of inorganic NCs passivated with nucleophilic amines.

## Supplementary Material

Refer to Web version on PubMed Central for supplementary material.

## Acknowledgements

We thank Simone Lauciello and Dr Rosaria Brescia (IIT Electron Microscopy Facility) for the assistance with EDS measurements; Mr Aniruddha Ray and Dr Ahmed Abdelhady for providing samples of bulk $Cs_4PbBr_6$ powders for

the control experiments; Dr Urko Petralanda, Dr Ivan Infante, and Mr Stefano Toso for helpful discussions; Dr Luana Persano for support in optical measurements and film sample preparation. The work of Dmitry Baranov was supported by the European Union's Horizon 2020 Research and Innovation Programme under Marie Sklodowska-Curie grant agreement No 794560 (RETAIN). Liberato Manna acknowledges funding from the European Union under grant agreement No 614897 (ERC Grant TRANSNANO). Riccardo Scarfiello acknowledges financial support by the Progetto FISR – C.N.R,"Tecnopolo di nanotecnologia e fotonica per la medicina di precisione" – CUP B83B17000010001. Andrea Camposeo and Dario Pisignano acknowledge funding from the European Research Council under the European Union's Horizon 2020 Research and Innovation Programme (Grant Agreement n. 682157, "*x*PRINT"), and from MIUR (project "3D-Phys", PRIN 2017PHRM8X).

## Abbreviations

| | |
|---|---|
| **COD** | Crystallography open database |
| **EDS** | Energy dispersive X-ray spectroscopy |
| **FFT** | Fast Fourier transform |
| **FTIR** | Fourier transform infrared spectroscopy HRTEM High resolution TEM |
| **HSQC** | Heteronuclear single quantum coherence ICSD Inorganic crystal structure database |
| **NIR** | Near infrared |
| **NMR** | Nuclear magnetic resonance |
| **NC** | Nanocrystal |
| **PL** | Photoluminescence |
| **PMAO** | Poly(maleic anhydride-*alt*-1-octadecene) QY Quantum yield |
| **STEM** | Scanning TEM |
| **TEM** | Transmission electron microscopy |
| **XRD** | X-ray diffraction |

## References

1. Kovalenko MV, Protesescu L, Bodnarchuk MI. Properties and potential optoelectronic applications of lead halide perovskite nanocrystals. Science. 2017; 358(6364):745–750. [PubMed: 29123061]
2. Akkerman QA, Rainò G, Kovalenko MV, Manna L. Genesis, challenges and opportunities for colloidal lead halide perovskite nanocrystals. Nat Mater. 2018; 17(5):394–405. [PubMed: 29459748]
3. Shamsi J, Urban AS, Imran M, De Trizio L, Manna L. Metal Halide Perovskite Nanocrystals: Synthesis, Post-Synthesis Modifications, and Their Optical Properties. Chem Rev. 2019; 119(5):3296–3348. [PubMed: 30758194]
4. Nedelcu G, Protesescu L, Yakunin S, Bodnarchuk MI, Grotevent MJ, Kovalenko MV. Fast Anion-Exchange in Highly Luminescent Nanocrystals of Cesium Lead Halide Perovskites ($CsPbX_3$, X =Cl, Br, I). Nano Lett. 2015; 15(8):5635–5640. [PubMed: 26207728]
5. Protesescu L, Yakunin S, Bodnarchuk MI, Krieg F, Caputo R, Hendon CH, Yang RX, Walsh A, Kovalenko MV. Nanocrystals of Cesium Lead Halide Perovskites ($CsPbX_3$, X = Cl, Br, and I):

Europe PMC Funders Author Manuscripts

Novel Optoelectronic Materials Showing Bright Emission with Wide Color Gamut. Nano Lett. 2015; 15(6):3692–3696. [PubMed: 25633588]

6. Akkerman QA, D'Innocenzo V, Accornero S, Scarpellini A, Petrozza A, Prato M, Manna L. Tuning the Optical Properties of Cesium Lead Halide Perovskite Nanocrystals by Anion Exchange Reactions. J Am Chem Soc. 2015; 137(32):10276–10281. [PubMed: 26214734]
7. Akkerman QA, Park S, Radicchi E, Nunzi F, Mosconi E, De Angelis F, Brescia R, Rastogi P, Prato M, Manna L. Nearly Monodisperse Insulator $Cs_4PbX_6$ (X = Cl, Br, I) Nanocrystals, Their Mixed Halide Compositions, and Their Transformation into $CsPbX_3$ Nanocrystals. Nano Lett. 2017; 17(3):1924–1930. [PubMed: 28196323]
8. Liu Z, Bekenstein Y, Ye X, Nguyen SC, Swabeck J, Zhang D, Lee S-T, Yang P, Ma W, Alivisatos AP. Ligand Mediated Transformation of Cesium Lead Bromide Perovskite Nanocrystals to Lead Depleted $Cs_4PbBr_6$ Nanocrystals. J Am Chem Soc. 2017; 139(15):5309–5312. [PubMed: 28358191]
9. Palazon F, Urso C, De Trizio L, Akkerman Q, Marras S, Locardi F, Nelli I, Ferretti M, Prato M, Manna L. Postsynthesis Transformation of Insulating $Cs_4PbBr_6$ Nanocrystals into Bright Perovskite $CsPbBr_3$ through Physical and Chemical Extraction of CsBr. ACS Energy Lett. 2017; 2(10):2445–2448. [PubMed: 29285525]
10. Udayabhaskararao T, Houben L, Cohen H, Menahem M, Pinkas I, Avram L, Wolf T, Teitelboim A, Leskes M, Yaffe O, Oron D, et al. A Mechanistic Study of Phase Transformation in Perovskite Nanocrystals Driven by Ligand Passivation. Chem Mater. 2018; 30(1):84–93.
11. Li Y, Huang H, Xiong Y, Kershaw SV, Rogach AL. Reversible transformation between $CsPbBr_3$ and $Cs_4PbBr_6$nanocrystals. CrystEngComm. 2018; 20(34):4900–4904.
12. Wu L, Hu H, Xu Y, Jiang S, Chen M, Zhong Q, Yang D, Liu Q, Zhao Y, Sun B, Zhang Q, et al. From Nonluminescent $Cs_4PbX_6$(X = Cl, Br, I) Nanocrystals to Highly Luminescent $CsPbX_3$Nanocrystals: Water-Triggered Transformation through a CsX-Stripping Mechanism. Nano Lett. 2017; 17(9):5799–5804. [PubMed: 28806517]
13. Hu H, Wu L, Tan Y, Zhong Q, Chen M, Qiu Y, Yang D, Sun B, Zhang Q, Yin Y. Interfacial Synthesis of Highly Stable $CsPbX_3$/Oxide Janus Nanoparticles. J Am Chem Soc. 2018; 140(1):406–412. [PubMed: 29228773]
14. Yang L, Wang T, Min Q, Liu B, Liu Z, Fan X, Qiu J, Xu X, Yu J, Yu X. High Water Resistance of Monoclinic $CsPbBr_3$Nanocrystals Derived from Zero-Dimensional Cesium Lead Halide Perovskites. ACS Omega. 2019; 4(3):6084–6091.
15. Chen M, Hu H, Tan Y, Yao N, Zhong Q, Sun B, Cao M, Zhang Q, Yin Y. Controlled growth of dodecapodbranched $CsPbBr_3$nanocrystals and their application in white light emitting diodes. Nano Energy. 2018; 53:559–566.
16. Wei Y, Cheng Z, Lin J. An overview on enhancing the stability of lead halide perovskite quantum dots and their applications in phosphor-converted LEDs. Chem Soc Rev. 2019; 48(1):310–350. [PubMed: 30465675]
17. Raja SN, Bekenstein Y, Koc MA, Fischer S, Zhang D, Lin L, Ritchie RO, Yang P, Alivisatos AP. Encapsulation of Perovskite Nanocrystals into Macroscale Polymer Matrices: Enhanced Stability and Polarization. ACS Appl Mater Interfaces. 2016; 8(51):35523–35533. [PubMed: 27991752]
18. Rainò G, Landuyt A, Krieg F, Bernasconi C, Ochsenbein ST, Dirin DN, Bodnarchuk MI, Kovalenko MV. Underestimated Effect of a Polymer Matrix on the Light Emission of Single $CsPbBr_3$Nanocrystals. Nano Lett. 2019; 19(6):3648–3653. [PubMed: 31117751]
19. Wang Y, Zhu Y, Huang J, Cai J, Zhu J, Yang X, Shen J, Jiang H, Li C. $CsPbBr_3$Perovskite Quantum Dots-Based Monolithic Electrospun Fiber Membrane as an Ultrastable and Ultrasensitive Fluorescent Sensor in Aqueous Medium. J Phys Chem Lett. 2016; 7(21):4253–4258. [PubMed: 27734662]
20. Kim H, So S, Ribbe A, Liu Y, Hu W, Duzhko VV, Hayward RC, Emrick T. Functional polymers for growth and stabilization of $CsPbBr_3$perovskite nanoparticles. Chem Commun. 2019; 55(12):1833–1836.
21. Kim H, Hight-Huf N, Kang J-H, Bisnoff P, Sundararajan S, Thompson T, Barnes M, Hayward R, Emrick TS. Polymer Zwitterions for Stabilization of $CsPbBr_3$Perovskite Nanoparticle and Nanocomposite Films. Angew Chem Int Ed.

22. Pellegrino T, Manna L, Kudera S, Liedl T, Koktysh D, Rogach AL, Keller S, Rädler J, Natile G, Parak WJ. Hydrophobic Nanocrystals Coated with an Amphiphilic Polymer Shell: A General Route to Water Soluble Nanocrystals. Nano Lett. 2004; 4(4):703–707.
23. Lin C-AJ, Sperling RA, Li JK, Yang T-Y, Li P-Y, Zanella M, Chang WH, Parak WJ. Design of an Amphiphilic Polymer for Nanoparticle Coating and Functionalization. Small. 2008; 4(3):334–341. [PubMed: 18273855]
24. Di Corato R, Quarta A, Piacenza P, Ragusa A, Figuerola A, Buonsanti R, Cingolani R, Manna L, Pellegrino T. Water solubilization of hydrophobic nanocrystals by means of poly(maleic anhydride-*alt*-1-octadecene). J Mater Chem. 2008; 18(17):1991–1996.
25. Almeida G, Goldoni L, Akkerman Q, Dang Z, Khan AH, Marras S, Moreels I, Manna L. Role of Acid-Base Equilibria in the Size, Shape, and Phase Control of Cesium Lead Bromide Nanocrystals. ACS Nano. 2018; 12(2):1704–1711. [PubMed: 29381326]
26. Rodà C, Abdelhady AL, Shamsi J, Lorenzon M, Pinchetti V, Gandini M, Meinardi F, Manna L, Brovelli S. $O_2$as a molecular probe for nonradiative surface defects in $CsPbBr_3$perovskite nanostructures and single crystals. Nanoscale. 2019; 11(16):7613–7623. [PubMed: 30964499]
27. Veáazquez M, Ferrier A, Péchev S, Gravereau P, Chaminade J-P, Portier X, Moncorgé R. Growth and characterization of pure and $Pr^{3+}$-doped $Cs_4PbBr_6$crystals. J Cryst Growth. 2008; 310(24):5458–5463.
28. Stoumpos CC, Malliakas CD, Peters JA, Liu Z, Sebastian M, Im J, Chasapis TC, Wibowo AC, Chung DY, Freeman AJ, Wessels BW, et al. Crystal Growth of the Perovskite Semiconductor $CsPbBr_3$: A New Material for High-Energy Radiation Detection. Cryst Growth Des. 2013; 13(7):2722–2727.
29. Kluger R, Hunt JC. Aminolysis of maleic anhydride. Kinetics and thermodynamics of amide formation. J Am Chem Soc. 1984; 106(19):5667–5670.
30. Kluger R, Hunt JC. Circumventive catalysis: contrasting reaction patterns of tertiary and primary amines with cyclic anhydrides and the avoidance of intermediates. J Am Chem Soc. 1989; 111(9):3325–3328.
31. Jin Z, Du L, Zhang C, Sugiyama Y, Wang W, Palui G, Wang S, Mattoussi H. Modification of Poly(maleic anhydride)-Based Polymers with $H_2N$-R Nucleophiles: Addition or Substitution Reaction? Bioconjugate Chem. 2019; 30(3):871–880.
32. Coleman L, Bork J, Dunn H. Notes. Reaction of Primary Aliphatic Amines with Maleic Anhydride. J Org Chem. 1959; 24(1):135–136.
33. Vermeesch I, Groeninckx G. Chemical modification of poly(styrene-co-maleic anhydride) with primary N-alkylamines by reactive extrusion. J Appl Polym Sci. 1994; 53(10):1365–1373.
34. De Roo J, Ibáñez M, Geiregat P, Nedelcu G, Walravens W, Maes J, Martins JC, Van Driessche I, Kovalenko MV, Hens Z. Highly Dynamic Ligand Binding and Light Absorption Coefficient of Cesium Lead Bromide Perovskite Nanocrystals. ACS Nano. 2016; 10(2):2071–2081. [PubMed: 26786064]
35. Bodnarchuk MI, Boehme SC, ten Brinck S, Bernasconi C, Shynkarenko Y, Krieg F, Widmer R, Aeschlimann B, Günther D, Kovalenko MV, Infante I. Rationalizing and Controlling the Surface Structure and Electronic Passivation of Cesium Lead Halide Nanocrystals. ACS Energy Lett. 2019; 4(1):63–74. [PubMed: 30662955]
36. Quarta D, Imran M, Capodilupo A-L, Petralanda U, van Beek B, De Angelis F, Manna L, Infante I, De Trizio L, Giansante C. Stable Ligand Coordination at the Surface of Colloidal $CsPbBr_3$Nanocrystals. J Phys Chem Lett. 2019; 10(13):3715–3726. [PubMed: 31244273]
37. Watanabe S, Kawahara H, Kuramochi T. Adducts of cyclic acid anhydrides and fatty amines as anti-rust additives in water-based cutting fluids. J Am Oil Chem Soc. 1991; 68(2):92–94.
38. Abbas M, Slugovc C. Optimized reaction conditions for the cross-metathesis of methyl oleate and oleylamine with ethyl acrylate. Monatsh Chem. 2012; 143(4):669–673.
39. Percec S, Howe L, Li J, Bair S. Chemical modification of poly(ethylene-co-methyl acrylate-co-maleic anhydride) for cathodic electrodepositions. J Polym Sci, Part A: Polym Chem. 2012; 50(2):261–270.
40. Zhang C, Gao C, Gao F, Wang J, Zhang D, Wang Y, Xu D. Synthesis of comb bipolymers and their pour point depressing properties. Pet Sci. 2014; 11(1):155–160.

41. Almeida G, Ashton OJ, Goldoni L, Maggioni D, Petralanda U, Mishra N, Akkerman QA, Infante I, Snaith HJ, Manna L. The Phosphine Oxide Route toward Lead Halide Perovskite Nanocrystals. J Am Chem Soc. 2018; 140(44):14878–14886. [PubMed: 30358392]
42. Park S, An NM, Almeida G, Palazon F, Spirito D, Krahne R, Dang Z, De Trizio L, Manna L. $CsPbX_3/SiO_x$(X=Cl, Br, I) Monoliths Prepared via a Novel Sol-gel Route Starting from $Cs_4PbX_6$Nanocrystals. Nanoscale. 2019; 11(40):18739–18745. [PubMed: 31591610]
43. Liu Y, Wang Z, Liang S, Li Z, Zhang M, Li H, Lin Z. Polar Organic Solvent-Tolerant Perovskite Nanocrystals Permanently Ligated with Polymer Hairs via Star-like Molecular Bottlebrush Trilobe Nanoreactors. Nano Lett. 2019; 19(12):9019–9028. [PubMed: 31692361]
44. Meyns M, Peáalvarez M, Heuer-Jungemann A, Hertog W, Ibáñez M, Nafria R, Genç A, Arbiol J, Kovalenko MV, Carreras J, Cabot A, et al. Polymer-Enhanced Stability of Inorganic Perovskite Nanocrystals and Their Application in Color Conversion LEDs. ACS Appl Mater Interfaces. 2016; 8(30):19579–19586. [PubMed: 27454750]
45. Wu H, Wang S, Cao F, Zhou J, Wu Q, Wang H, Li X, Yin L, Yang X. Ultrastable Inorganic Perovskite Nanocrystals Coated with a Thick Long-Chain Polymer for Efficient White Light-Emitting Diodes. Chem Mater. 2019; 31(6):1936–1940.
46. Carrillo-Carrión C, del Pino P, Pelaz B. Aqueous stable luminescent perovskite-polymer composites. Applied Materials Today. 2019; 15:562–569.
47. Momma K, Izumi F. VESTA 3 for three-dimensional visualization of crystal, volumetric and morphology data. J Appl Crystallogr. 2011; 44(6):1272–1276.
48. Wright AD, Verdi C, Milot RL, Eperon GE, Pérez-Osorio MA, Snaith HJ, Giustino F, Johnston MB, Herz LM. Electron-phonon coupling in hybrid lead halide perovskites. Nat Commun. 2016; 7(1)
49. Guo Y, Yaffe O, Hull TD, Owen JS, Reichman DR, Brus LE. Dynamic emission Stokes shift and liquid-like dielectric solvation of band edge carriers in lead-halide perovskites. Nat Commun. 2019; 10(1)
50. Nikl M, Mihokova E, Nitsch K, Somma F, Giampaolo C, Pazzi GP, Fabeni P, Zazubovich S. Photoluminescence of $Cs_4PbBr_6$crystals and thin films. Chem Phys Lett. 1999; 306(5):280–284.
51. Babin V, Fabeni P, Mihokova E, Nikl M, Pazzi GP, Zazubovich N, Zazubovich S. Luminescence of $Cs_4PbBr_6$Aggregates in As-Grown and in Annealed CsBr:Pb Single Crystals. Phys Status Solidi B. 2000; 219(1):205–214.
52. Radhakrishna S, Pande KP. Lead Centers in Cesium Halides. Phys Rev B. 1973; 7(1):424–431.
53. Jacobs PWM. Alkali halide crystals containing impurity ions with the $ns^2$ ground-state electronic configuration. J Phys Chem Solids. 1991; 52(1):35–67.
54. Yin J, Zhang Y, Bruno A, Soci C, Bakr OM, Bédas J-L, Mohammed OF. Intrinsic Lead Ion Emissions in Zero-Dimensional $Cs_4PbBr_6$Nanocrystals. ACS Energy Lett. 2017; 2(12):2805–2811.
55. Hoy J, Morrison PJ, Steinberg LK, Buhro WE, Loomis RA. Excitation Energy Dependence of the Photoluminescence Quantum Yields of Core and Core/Shell Quantum Dots. J Phys Chem Lett. 2013; 4(12):2053–2060. [PubMed: 26283252]
56. Imran M, Caligiuri V, Wang M, Goldoni L, Prato M, Krahne R, De Trizio L, Manna L. Benzoyl Halides as Alternative Precursors for the Colloidal Synthesis of Lead-Based Halide Perovskite Nanocrystals. J Am Chem Soc. 2018; 140(7):2656–2664. [PubMed: 29378131]
57. Imran M, Ijaz P, Baranov D, Goldoni L, Petralanda U, Akkerman Q, Abdelhady AL, Prato M, Bianchini P, Infante I, Manna L. Shape-Pure, Nearly Monodispersed $CsPbBr_3$Nanocubes Prepared Using Secondary Aliphatic Amines. Nano Lett. 2018; 18(12):7822–7831. [PubMed: 30383965]
58. Imran M, Ijaz P, Goldoni L, Maggioni D, Petralanda U, Prato M, Almeida G, Infante I, Manna L. Simultaneous Cationic and Anionic Ligand Exchange For Colloidally Stable $CsPbBr_3$Nanocrystals. ACS Energy Lett. 2019; 4(4):819–824.
59. Wang Y, He J, Chen H, Chen J, Zhu R, Ma P, Towers A, Lin Y, Gesquiere AJ, Wu S-T, Dong Y. Ultrastable, Highly Luminescent Organic-Inorganic Perovskite-Polymer Composite Films. Adv Mater. 2016; 28(48):10710–10717. [PubMed: 27748549]

60. Yoon SJ, Guo Z, dos Santos Claro PC, Shevchenko EV, Huang L. Direct Imaging of Long-Range Exciton Transport in Quantum Dot Superlattices by Ultrafast Microscopy. ACS Nano. 2016; 10(7):7208–7215. [PubMed: 27387010]

61. Dujardin C, Auffray E, Bourret-Courchesne E, Dorenbos P, Lecoq P, Nikl M, Vasil'ev AN, Yoshikawa A, Zhu R. Needs, Trends, and Advances in Inorganic Scintillators. IEEE Trans Nucl Sci. 2018; 65(8):1977–1997.

62. Tomanová K, Čuba V, Brik MG, Mihóková E, Turtos RM, Lecoq P, Auffray E, Nikl M. On the structure, synthesis, and characterization of ultrafast blue-emitting $CsPbBr_3$ nanoplatelets. APL Mater. 2019; 7(1)



Europe PMC Funders Author Manuscripts

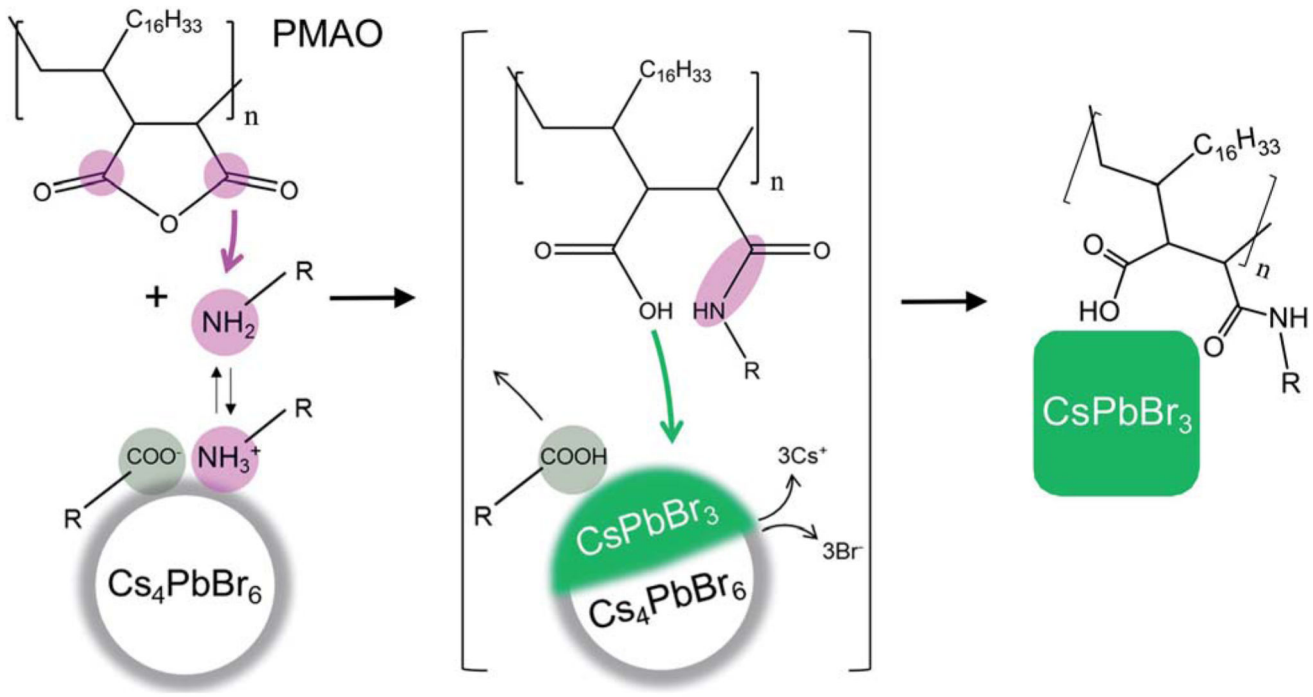


**Fig. 1.**

Schematic representation of the $Cs_4PbBr_6 \rightarrow CsPbBr_3$ NC transformation induced by PMAO. Oleylamine species from the NC surface react with the cyclic anhydride rings of PMAO, forming polysuccinamic acid. The removal of oleylamine-based and oleate ligands destabilizes the NC surface, and the formation of polysuccinamic acid increases the acidity of the medium, triggering the $Cs4PbBr_6 \rightarrow CsPbBr_3$ transformation (see the text for the chemical equation). The resulting $CsPbBr_3$ NCs are stabilized by the polysuccinamic acid in place of the original ligands.




Europe PMC Funders Author Manuscripts

Europe PMC Funders Author Manuscripts

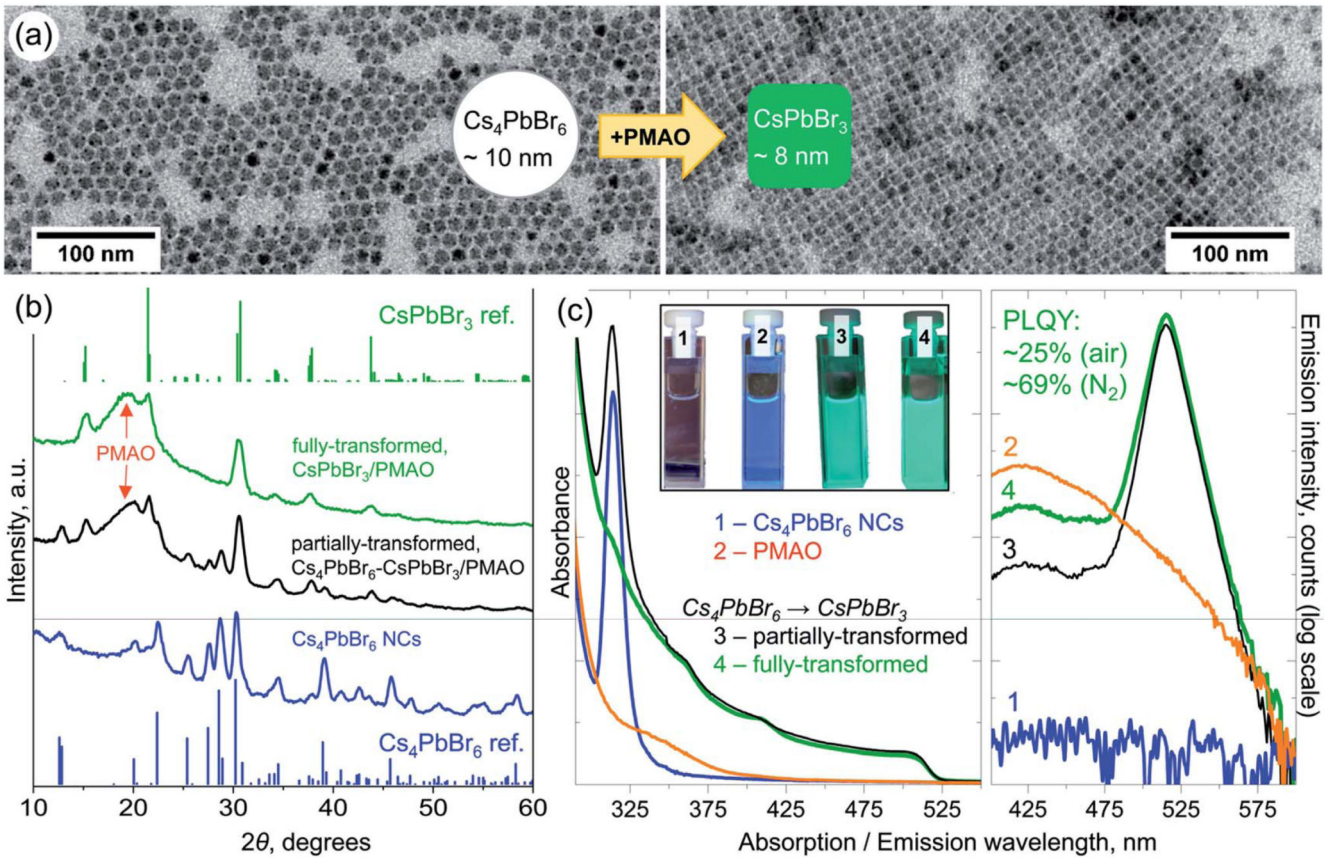


**Fig. 2.**

(a) Low-magnification TEM images of the initial $Cs_4PbBr_6$ NCs (average diameter 10 ± 1.5 nm) and fully-transformed $CsPbBr_3$ NCs (average edge length 8 ± 0.4 nm) after their reaction with PMAO in toluene. (b) XRD patterns of the initial $Cs_4PbBr_6$ NCs and of the partially- and fully-transformed ones. Top and bottom stick patterns are those of the reference bulk compounds: rhombohedral $Cs_4PbBr_6$ (pattern ID 04-015-9683, ICSD code 162158)[27] and orthorhombic $CsPbBr_3$ (pattern ID 96-451-0746, COD code 4510745).[28] The broad peak at ~20 °is due to PMAO. (c) Optical absorption (left panel) and emission (right panel) spectra of toluene solutions of initial $Cs_4PbBr_6$ NCs (blue curve), PMAO (orange curve), and partially- (black curve), and fully-transformed (green curve) NCs. The inset in the left panel shows photographs of the samples under excitation with a 365 nm lamp demonstrating visible green PL of partially- and fully-transformed NC samples.

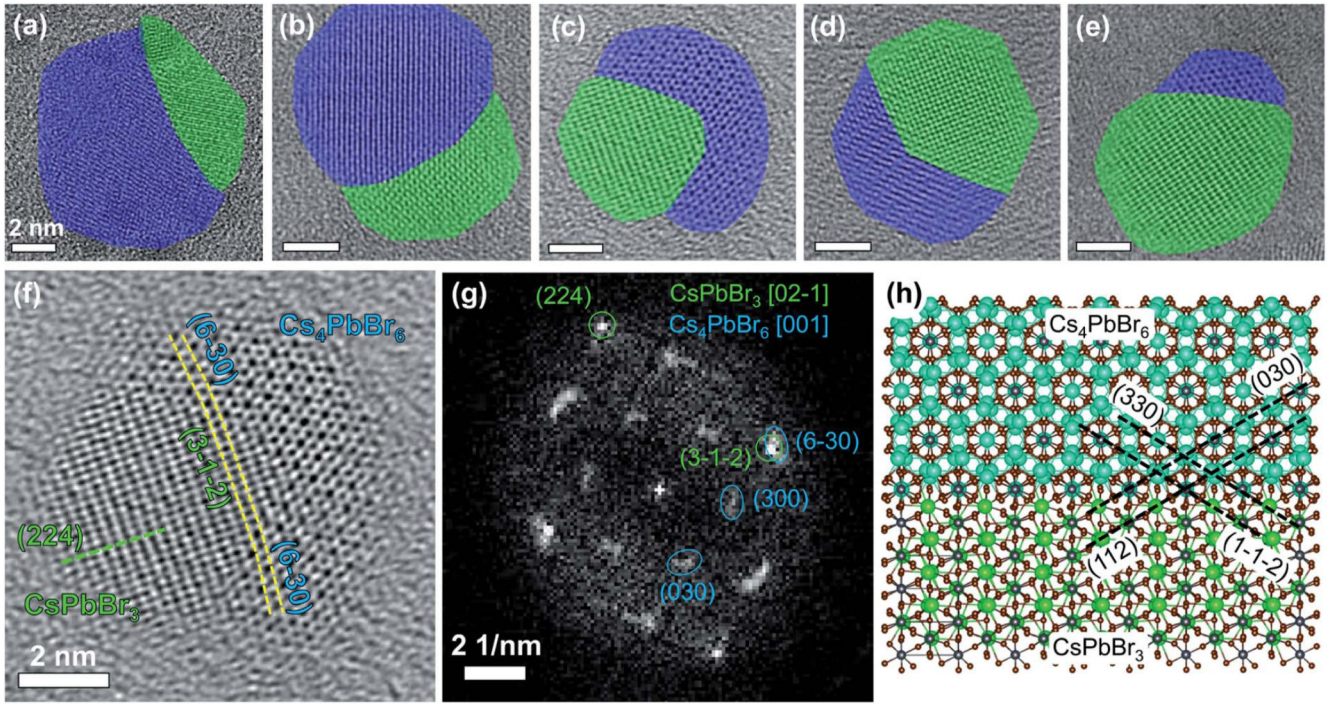


**Fig. 3.**

(a–e) HRTEM images of $Cs_4PbBr_6$–$CsPbBr_3$ heterostructures formed upon partial conversion of $Cs_4PbBr_6$ NCs with PMAO (scale bars are 2 nm). $Cs_4PbBr_6$ domains are shaded in blue, and $CsPbBr_3$ domains are shaded in green; (f) a magnified view of (c) and (g) the corresponding FFT image; and (h) ball-and-stick atomic model of the epitaxial interface built using VESTA software (ver. 3.4.6, the atoms are depicted as spheres with radii corresponding to 40% of actual atomic radii).[47] Cs atoms in the model are colored in two different colors for clarity: in cyan for $Cs_4PbBr_6$ and green for $CsPbBr_3$.

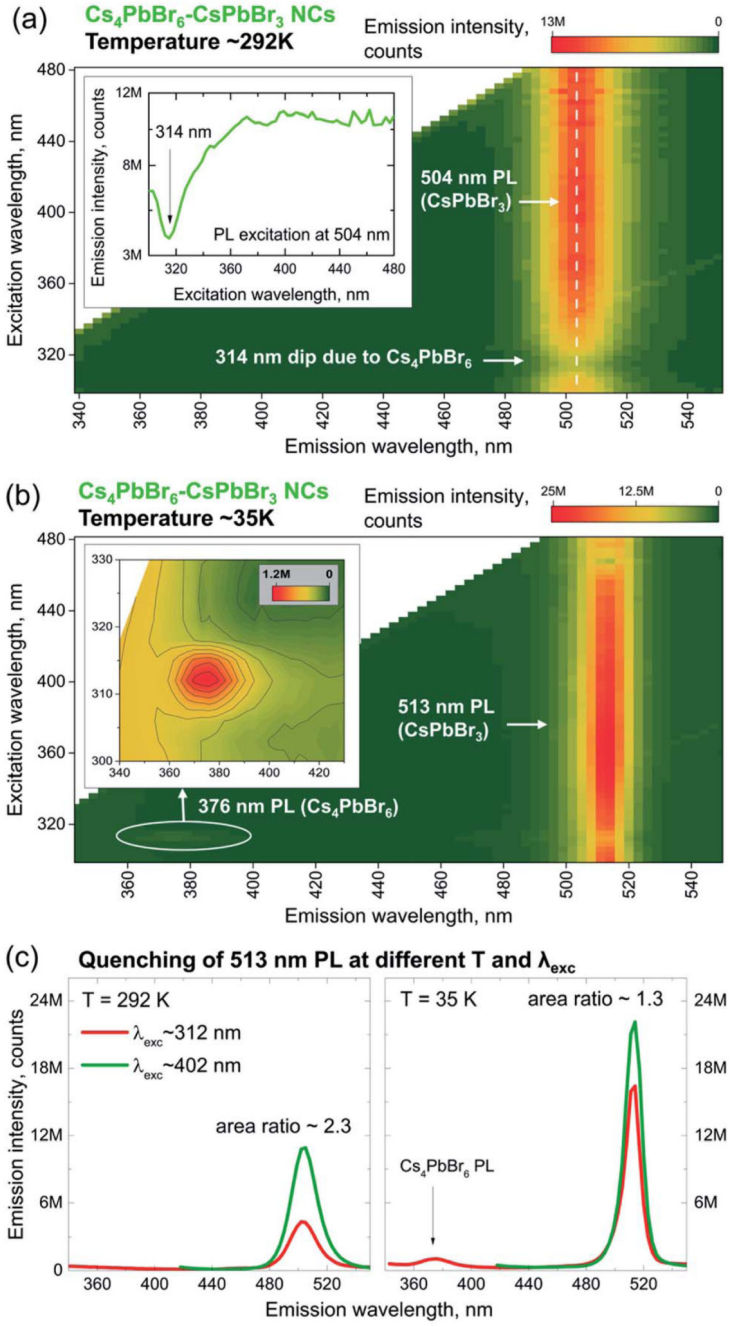


**Fig. 4.**

PL maps of (a) partially-transformed $Cs_4PbBr_6$–$CsPbBr_3$ NCs at room temperature, and the inset shows the PL excitation spectrum at ~504 nm (indicated by a white dashed line in the PL map); (b) partially-transformed $Cs_4PbBr_6$–$CsPbBr_3$ NCs at ~35 K, and the inset shows the low intensity region around 376 nm; (c) PL spectra of $Cs_4PbBr_6$–$CsPbBr_3$ NCs at 292 K (left panel) and 35 K (right panel) collected under ~312 nm (red curve) and ~402 nm (green curve) excitation.

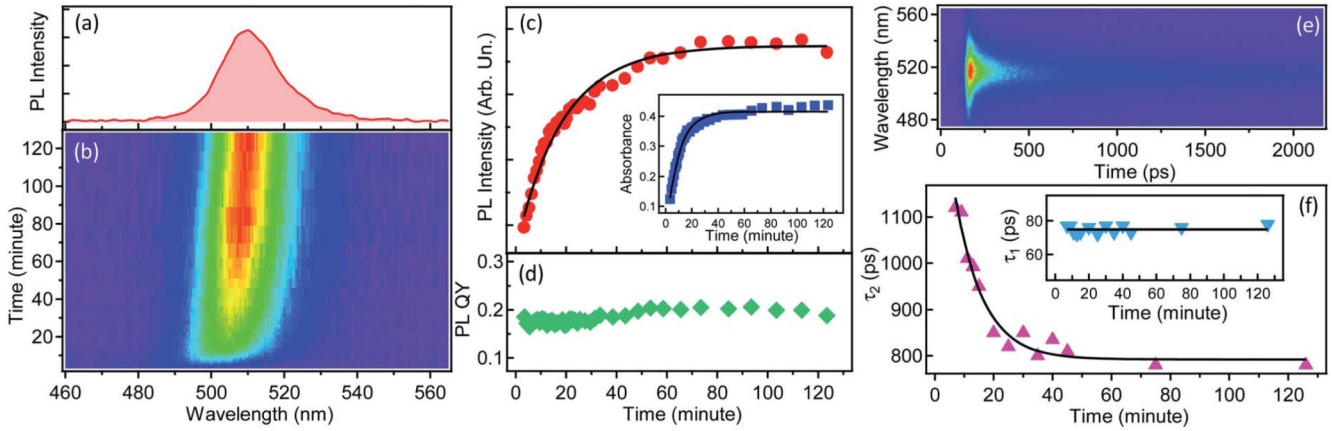


**Fig. 5.**

Tracking the $Cs_4PbBr_6 \rightarrow CsPbBr_3$ NC transformation in a drop-cast film by PL spectroscopy. (a) PL spectrum of the fully transformed $CsPbBr_3$ NCs, peaking at ~510 nm. (b) Spectrally-resolved temporal evolution of the PL spectrum on a minute scale, for ~120 minutes. (c) Time evolution of the integrated PL intensity fitted with first-order kinetics (solid black line, time ~10 min). The inset shows time-dependent absorbance at 405 nm over the course of the transformation. (d) Time-dependent PLQY of the drop-cast film. (e) PL intensity map showing the picosecond temporal behavior of the emission intensity of the drop-cast films. (f) Temporal evolution of the longer PL decay lifetime, $\tau_2$, over the NCs transformation. The continuous line is a fit to the data by first-order kinetics. The corresponding trend for the shorter component, $\tau_1$, is shown in the inset.




Europe PMC Funders Author Manuscripts